GeoScienceWorld
Lithosphere
Volume 2020, Article ID 7866789, 17 pages
https://doi.org/10.2113/2020/7866789

Lithosphere

Research Article

Tectonochemistry of the Brooks Range Ophiolite, Alaska

Joseph Biasi,[1] **Paul Asimow**,[1] **and Ronald Harris**[2]

[1]*Division of Geological and Planetary Sciences, California Institute of Technology, 1200 E. California Blvd., Pasadena, CA 91125, USA*
[2]*Department of Geological Sciences, Brigham Young University, S389 Eyring Science Center, Provo, Utah 84602, USA*

Correspondence should be addressed to Joseph Biasi; biasi@caltech.edu

Received 23 September 2020; Accepted 7 December 2020; Published 24 December 2020

Academic Editor: Sarah Brownlee

We present new whole-rock geochemical data from the Brooks Range ophiolite (BRO) together with new mineral chemistry data from the BRO, South Sandwich forearc, Izu-Bonin forearc, and Hess Deep. The analyses reveal that the Brooks Range ophiolite (BRO) was most likely created in a forearc setting. We show that this tectonic classification requires the Brookian orogeny to begin at ~163-169 Ma. The middle-Jurassic BRO contains abundant gabbros and other intrusive rocks that are geochemically similar to lithologies found in other forearc settings. Based on major, minor, and trace element geochemistry, we conclude that the BRO has clear signals of a subduction-related origin. High-precision olivine data from the BRO have a forearc signature, with possible geochemical input from a nearby arc. The Koyukuk terrane lies to the south of the Brooks Range; previous studies have concluded that the BRO is the forearc remnant of this arc-related terrane. These studies also conclude that collision between the Koyukuk Arc and the Arctic Alaska continental margin marks the beginning of the Brookian orogeny. Since the BRO is a forearc ophiolite, the collision between the Koyukuk Arc and the continental margin must have coincided with obduction of the BRO. Previously determined $^{40}Ar/^{39}Ar$ ages from the BRO's metamorphic sole yield an obduction age of 163-169 Ma. Since the same collisional event that obducts the BRO also is responsible for the Brookian orogeny, we conclude that the BRO's obduction age of ~163-169 Ma marks the beginning of this orogenic event.

1. Introduction

Subduction is one of the defining processes that allows plate tectonics to operate and thereby determines the whole character of our planet. It is now well established that the majority of ophiolites are produced via subduction-related processes [1]. Although our understanding of suprasubduction zone (SSZ) ophiolites has advanced greatly over the last 30 years—due in part to ocean-drilling campaigns (e.g., [2, 3])—many aspects of these ophiolites are still poorly understood. This is especially true when it comes to processes occurring below the extrusive layer.

In the North American Cordillera, most ophiolites have experienced complex syn- and postemplacement deformation and alteration [4]. This greatly complicates their geochemical characterization, which is required to identify the tectonic setting in which they are generated [5]. Previous studies of *in situ* forearcs, arcs, and back-arcs have mostly focused on the extrusive layer (pillow basalts and sheeted dikes), as the extrusive section is readily sampled by seafloor drilling and features characteristic rock types such as boninites and forearc basalts (e.g., [6]). It therefore follows that most tectonochemical indicators for ophiolites and seafloor basalts have been developed with the extrusive layer in mind [5].

In this study, we present novel geochemical data from the Brooks Range ophiolite, South Sandwich forearc, Izu-Bonin forearc, and Hess Deep. With these data, we show that the *intrusive* section of the Brooks Range ophiolite (BRO) (Figure 1) in northern Alaska preserves a forearc geochemical signature. We then use the forearc model of the BRO to resolve several outstanding issues regarding the Mesozoic tectonic history of northern Alaska. Notably, the tectonic history of the BRO requires that the Brookian orogeny begin at ~163-169 Ma, when the BRO is obducted onto the Arctic Alaska margin.

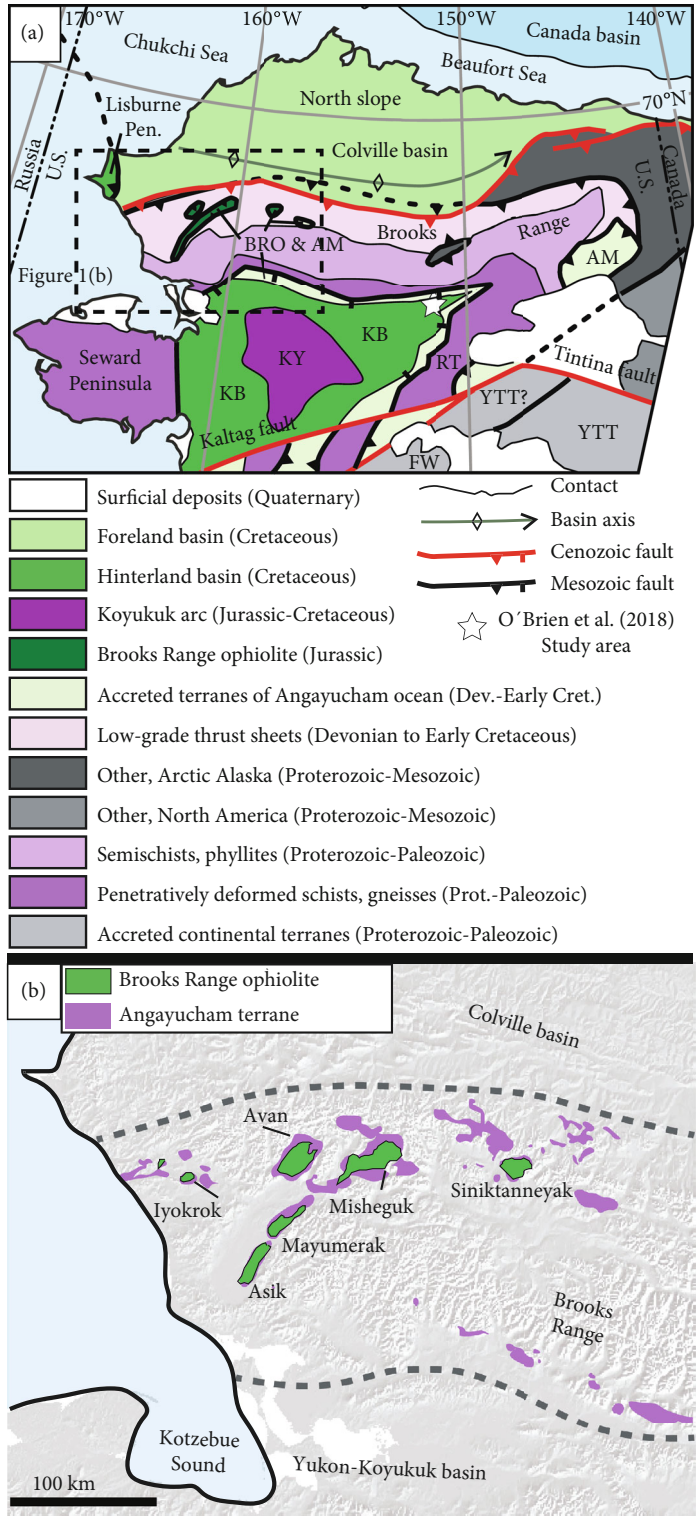

Figure 1: (a) Overview map showing major areas discussed in the text. Lightly modified from [42]. Abbreviations: AM—Angayucham terrane; BRO—Brooks Range ophiolite; KB—Yukon-Koyukuk basin; KY—Koyukuk Arc; FW—Farewell terrane; RT—Ruby terrane; YTT—Yukon-Tanana terrane. (b) Map of the western Brooks Range showing exposures of the Brooks Range ophiolite (green) and Angayucham terrane (purple). The dashed lines mark the approximate boundaries of the Brooks Range. Based on maps by Wilson et al. [66] and Harris [7].

2. Geological Background

2.1. Brooks Range Ophiolite (BRO). The Brooks Range ophiolite (BRO) lies in northwestern Alaska (Figure 1), and is likely middle-Jurassic in age [7]. As it is currently (and conservatively) mapped, the BRO covers 1800 km^2. It is composed of six klippe-like massifs. Most studies have focused on three of these massifs (Misheguk, Avan, and Siniktanneyak) [7]. Complete ophiolitic sections (from metamorphic sole to pillow basalts/chert) can be found in these three massifs. Glacial erosion of the ophiolite bodies provides nearly 100% exposure in many places.

Only a handful of papers have been published on the BRO, and most studies were published pre-2000. Early reconnaissance-level studies of the western Brooks Range produced various models for the tectonic evolution of the BRO [8–18]. The most recent and thorough work on the BRO was done in the late 1980s and 1990s and focused mostly on the Siniktanneyak and Misheguk massifs [7, 19–22]. This work mainly involved structural mapping, petrology, and age analysis. Some major and trace element geochemical data were also reported. Hornblende $^{40}Ar/^{39}Ar$ plateau ages were reported for gabbro and metamorphic sole rocks from the Avan, Asik, Misheguk, and Siniktanneyak massifs. The conclusions most relevant to this study are as follows:

(1) The Brooks Range ophiolite contains a complete section of oceanic lithosphere composed, from bottom to top, of a metamorphic sole with partial melts, dunitic and harzburgitic peridotite (serpentinized near the sole but otherwise pristine), transitional ultramafic cumulates (petrologic Moho), thick sections (~4 km) of layered gabbro, massive gabbro, intermediate intrusives, ultramafic/mafic late-stage intrusives, sheeted dikes, pillow basalts, and sedimentary deposits [7]

(2) The geochemistry of the BRO is most consistent with formation in an SSZ setting, followed by obduction during arc-continent collision and incorporation into the Brooks Range fold-and-thrust belt [20]

(3) The metamorphic sole beneath the BRO is composed mostly of Angayucham (Copter Peak) basalt and intercalated sedimentary rocks. The geochemistry and age of these basalts precludes any genetic relations between them and the BRO [21]

(4) The BRO is at the structurally highest position in the Brooks Range, and strain was localized in the serpentinized structural base of the ophiolite and its metamorphic sole during emplacement. Due to these factors, the BRO has remained mostly intact and was subjected only to typical seafloor deformation and alteration [21]

Previous studies suggest that the BRO is comprised of suprasubduction zone (SSZ) lithosphere associated with early development of the Koyukuk Arc, a fossil arc terrane situated today south of the Brooks Range (Figure 1) (e.g., [7, 21]). Arc-continent collision between the Koyukuk Arc and the Arctic Alaska continental margin probably led to obduction of the BRO [19, 21, 23].

$^{40}Ar/^{39}Ar$ plateau ages are interpreted to give overlapping cooling ages of 163 – 169 ± 5 Ma for both the BRO and its metamorphic sole [7, 24, 25]. Such overlap is a common characteristic among SSZ ophiolites with a metamorphic sole [19]. U-Pb zircon data from late-stage BRO melts yield an age of 170 ± 3 Ma [26]. This age is within error of $^{40}Ar/^{39}Ar$ ages from BRO gabbro and the metamorphic sole [7]. These geochronological constraints indicate that the BRO was obducted onto the Angayucham terrane shortly after formation. The BRO's quick obduction, combined with its structurally highest position in the Brooks Range, has allowed the ophiolite to remain only lightly serpentinized and avoid overprinting by postobduction events that commonly affect other Cordilleran ophiolites.

2.2. Other Oceanic Rocks. Typically, all Mesozoic oceanic rocks within the Brooks Range are referred to as the Angayucham terrane [27]. This terrane grouping, however, is somewhat misleading. The BRO has a suprasubduction zone origin [20], while the structurally underlying basalts have an oceanic plateau/MORB affinity [17, 19, 28, 29]. Some authors (e.g., [23]) have therefore divided the Angayucham terrane into the Misheguk Mountain Allochthon and the structurally underlying Copter Peak Allochthon. However, differences in age and geochemistry preclude any shared geologic history between these units prior to emplacement [21]. Further complicating the issue, many oceanic rocks in interior Alaska are also referred to as the Angayucham terrane (Figure 1) [30]. Ideally, the Angayucham terrane would be split into an arc-related terrane and a MORB-related terrane to reflect this. However, most areas of the Angayucham terrane lack sufficient geochemical and geochronological data for such a split to be viable, especially in the Alaskan interior.

For the purposes of this study, the Jurassic BRO and the rest of the Angayucham terrane are not the same, and therefore, we will always refer to the green areas in Figure 1(b) as "Brooks Range ophiolite (BRO)" and the structurally lower purple areas as "Angayucham." This distinction will be particularly relevant later in this paper.

Most of the initial mapping in the area was done via helicopter/aerial photography, and it is likely that large swaths of the BRO are incorrectly mapped as Angayucham, as discovered in the Siniktanneyak massif [7]. The Angayucham terrane structurally underlies the BRO but consists of similar lithologies (gabbro, pillow basalt, and chert). It locally makes up the BRO's metamorphic sole [19, 21] and was emplaced synchronously with the BRO. In our estimation, the BRO *could* currently cover as much as 3600 km^2. This makes it one of the largest, best exposed, and most complete ophiolites in the Western Hemisphere, yet relatively understudied.

2.3. Tectonics of Northern Alaska. The tectonic evolution of northern Alaska remains controversial, and a full review is beyond the scope of this work. A number of recent review papers cover the subject in detail (e.g., [31–35]). In brief,

since the breakup of Pangea, the Arctic region has experienced a poorly constrained series of tectonic shifts, rotations, and subduction events. The end result is that the area is now surrounded by blocks of continental crust with similar pre-Mesozoic histories, but divergent Mesozoic-Cenozoic histories [31, 36, 37].

One of these lithospheric blocks contains the Brooks Range (Figure 1). After initial mineral exploration in the 1960s and 1970s, little mapping has been done in the range and it remains among the least studied areas in North America. This situation is primarily due to its remote location and short summers. The range has experienced a revival in research interest in the last 10 years or so. The Brooks Range itself is composed of several accreted terranes [27, 38, 39], and is bordered by the Koyukuk terrane to the south and the North Slope subterrane (Colville basin) to the north (Figure 1). Many of these terranes have experienced multiple metamorphic and deformational events, but it is clear that in the early Jurassic the Brooks Range did not yet exist [23]. Instead, northern Alaska was a south-facing (in present-day coordinates) passive continental margin (referred to as "Arctic Alaska"), which transitioned into the Angayucham oceanic basin [19].

It is thought that an oceanic arc (likely the Koyukuk Arc) collided with the passive continental margin to initiate the Brookian orogeny along a south dipping subduction zone [19, 23, 35, 39, 40]. This model is similar to the presently active collision of the Banda Arc with the passive continental margin of northern Australia [19, 41]. In this model, the arc is not related to the continental margin in any way before collision. Other interpretations suggest the Koyukuk Arc was formed by northward subduction and was separated from Arctic Alaska by a (likely narrow) back-arc sea [11, 16, 42, 43]. The narrow sea or back-arc model for the BRO purports that sometime in the Jurassic or Cretaceous the back-arc basin closed as the Koyukuk Arc collided with Arctic Alaska.

Collision between the continental margin and the Koyukuk Arc marked the beginning of the Brookian orogeny [39, 44]. This collision must have occurred sometime in the Early Cretaceous or Late Jurassic, based on geochronological studies of metamorphism in the Brooks Range [35]. Precisely dating the onset of Brookian orogenesis has been an elusive goal for decades. Metamorphic rocks associated with this event have been difficult to date due to extensive Cretaceous greenschist-facies overprinting of the original blueschist-facies metamorphism [35, 45]. This metamorphic overprint is not unique to the Brooks Range. Many collisional belts yield metamorphic ages much younger than the early phases of associated ophiolite emplacement (e.g., Oman [46]).

A foreland basin (Colville, Figure 1) developed adjacent to the Brooks Range during orogenesis. Its lowest units consist of mélange with blocks of Angayucham terrane and Late Jurassic intermediate volcanics [47]. Overlying the mélange are synorogenic deposits containing Jurassic detrital zircons [23, 48] that likely originated from the BRO and underlying Angayucham terrane mafic rocks. This led Moore et al. [23] to conclude that the BRO and portions of the underlying Angayucham terrane were emplaced within the Colville basin watershed during Late Jurassic arc-continent collision. The Yukon-Koyukuk basin (YKB) (Figure 1(b)) currently does not expose any deposits older than Albian (i.e., latest Early Cretaceous). These units contain mafic lithic fragments and detrital zircons from 160 to 260 Ma. Clasts from these units have variable island-arc affinities, and have led researchers to recently conclude that a Late Triassic-Early Jurassic island arc was present in the area before the Albian [49]. It is possible that these clasts are derived from pre-BRO arc terranes, which may not have been near the continental margin at the time they formed. It is clear that the lowermost clasts from Jurassic Brookian foreland strata were derived from a different source than the Albian sediments accumulated in the YKB [49].

Geochronological data from the Koyukuk Arc is sparse. The Koyukuk Arc itself is dated via invertebrate fossils and the K-Ar method. On the basis of these fossil and isotopic ages, Box and Patton in 1989 divided the history of the Koyukuk Arc into four stages. The oldest lithologies (Stage 1) consist of late Paleozoic-early Mesozoic pillow basalt, chert, serpentinite, and limestone. Stage 2 consists of middle-Jurassic plutonic rocks (intermediate-felsic). Stages 3 and 4 consist of intermediate-felsic volcanic rocks, volcaniclastic sedimentary rocks, and shallow-deep marine sedimentary rocks. Stages 3 and 4 sedimentary rocks are early Cretaceous in age (<145 Ma) [15, 50]. Recent zircon ages from Koyukuk Arc plutonic rocks confirm that the arc was active during the Cretaceous [45].

This study presents evidence that the BRO was created in a forearc setting, which is a refinement of its earlier classification as an SSZ ophiolite [7, 20]. We will use this finding to determine the age of onset of Brookian orogenesis and develop a coherent tectonic model of the orogeny (see Discussion).

3. Methods

3.1. Fieldwork. Most samples used in this study were collected by R. A. Harris in 1986 and 1989 at Misheguk Massif (Figure 1(b)). Field descriptions of all units, geologic maps of several massifs, and detailed cross sections can be found in Ref. [7] and will not be reiterated here. The most relevant field observations for this study are that sheeted dikes and pillow basalts associated with the BRO are relatively rare. Most of the ophiolite is composed of intrusive and mantle lithologies. The intrusive lithologies include layered gabbro, massive gabbro, and high-level intermediate intrusives. The mantle lithologies consist mostly of dunite with abundant chromite and blebs or screens of harzburgite. Out-of-sequence mafic/ultramafic intrusives and plagiogranites can be found in any part of the ophiolitic section.

Three samples were collected by Lyle Nelson and Betsy Friedlander of Teck Resources in 2017. These samples are all mantle rocks from the Iyokrok massif, which is a small and poorly exposed klippe of the BRO. The entire Iyokrok massif consists of mantle lithologies and appears to be folded in a similar fashion to other BRO massifs [7].

3.2. Whole-Rock Geochemistry. New major oxide and minor element abundances were determined for 15 samples.

Samples with minimal petrographic evidence of metamorphism or serpentinization and only minor seafloor alteration were chosen, representing the common rock types within the BRO. All samples were analyzed using a Panalytical Zetium XRF system at the California Institute of Technology. Major and minor elements were analyzed using fused-glass beads. Following LOI determined at 1050°C, samples were mixed with 9 times their weight in 66.67% $Li_2B_4O_7$-32.83% $LiBO_2$-0.50% LiI flux and fused at 1200°C.

We also determined rare-earth element (REE) concentrations in 15 samples using an Agilent Technologies 8800 triple quadrupole ICP-MS. Chips (~25 mg) of the beads used for XRF analysis were dissolved in 50 mL polypropylene containers in 2 mL of hot (99°C) 3 : 1 nitric and hydrofluoric acid for 8 hours and diluted to 30 mL total volume with distilled water. To control for quality, four USGS standards (AGV-2, BCR-2, RGM-2, and DTS-2b) were included as unknowns. Whole-rock geochemical data (including detection limits and standards run as unknowns) are available in the Supplemental Information (Table S2).

3.3. Mineral Chemistry. Mineralogy and mineral chemistry were characterized for 33 polished sections. These sections were selected using the same criteria as the whole-rock samples. We employed a combination of Scanning Electron Microscopy (SEM) with Energy Dispersive X-ray Spectroscopy (EDS) and Electron Microprobe (EMP) analysis. Compositional maps were generated using SEM/EDS (Zeiss 1550 VP SEM operated at 15 kV, Oxford X-MAX Si-drift detector, Oxford AZtec software) to determine sample mineralogy, degree of serpentinization, and degree of metamorphism. EMP analyses (JEOL 8200 five-spectrometer instrument operated at 15 kV and 25 nA; synthetic and natural mineral and oxide standards; CITZAF data reduction) were used to determine the major-element chemistry of individual phases in each sample. High-precision analyses of olivine grains (JEOL 8200 five-spectrometer instrument operated at 20 kV and 300 nA; synthetic mineral and oxide standards; CITZAF data reduction, method of Sobolev et al. [51]) were also performed. During high-precision analysis, a San Carlos olivine crystal was analyzed before and after every sample and used as a drift correction standard. Mineral chemistry data is provided in the Supplemental Information (Tables S3, S4, S5, and S6).

4. Results

4.1. Samples and Context. We performed new analyses on 12 whole-rock samples collected by R. Harris at Misheguk massif (Figure 1(b)). Note that the samples were chosen to represent the wide array of rock types found in the BRO, and this translates to a wide array of compositions. Only one sample (a sheeted dike) was taken from the extrusive layer. The remaining sample set is from the intrusive section of the BRO. Misheguk is the largest massif in the BRO. The mantle section contains dunite, peridotite, transitional ultramafics, and late-stage ultramafic intrusions. The large crustal section contains layered gabbro (4 km stratigraphic thickness), massive gabbro, and high-level intermediate intrusives. See Ref. [7] for more detailed descriptions. We also analyzed 3 new ultramafic samples (whole-rock and thick-section) from the Iyokrok massif (Figure 1(b)). Whole-rock analyses of samples previously published from Siniktanneyak, Misheguk, and Avan massifs are also used in the study [20, 22]. In addition, 22 thin sections from Harris' 1986 and 1989 sample sets and 3 thick sections from Iyokrok were analyzed for mineral chemistry. Finally, 8 thin sections from the IBM forearc, South Sandwich forearc, and Hess Deep were analyzed using the high-precision olivine protocol described in Section 3.3. All mineral chemistry presented in this study is new.

4.2. Major, Minor, and Trace Elements. All new whole-rock oxide and elemental abundance data are reported in Table S2. The majority of discrimination diagrams typically used to assign the tectonic environment of igneous samples were developed for extrusive rocks. However, Baziotis et al. [52] showed that many of the relative trace element abundance characteristics of extrusive rocks are inherited from their parent liquids faithfully enough to apply tectonic discrimination diagrams, even though absolute concentrations of incompatible elements are lower in samples containing some cumulate component. Figure 2 shows new whole-rock data alongside published analyses by Harris [20] and Bickerstaff [22] in selected tectonic discrimination diagrams.

Samples from the crustal section of the BRO are shown in Figures 2(a) and 2(b). Samples that are clearly cumulates (layered gabbro, anorthosite, etc.) are excluded from these plots but reported in Table S2. Figure 2(a) makes use of two immobile elements for tectonic discrimination. All samples in this plot contain <55% SiO_2 to avoid evolved/cumulate samples. Many samples from Bickerstaff [22] do not have SiO_2 data and are not plotted here. Results show a range from boninitic to MORB affinity. Figure 2(b) also makes use of immobile elements and shows some boninitic samples in the dataset. The majority of crustal samples are not boninitic. Figures 2(c) and 2(d) show whole-rock geochemical results from the mantle section of the BRO. Figure 2(c) shows that these samples can be divided into two groups: cpx poor (harzburgite, dunite) and cpx bearing (wehrlite, pyroxenite, etc.). Finally, most harzburgites and dunites plot within the forearc peridotite field in Figure 2(d), though some samples may have a different tectonic affinity.

4.3. Rare-Earth Elements. New whole-rock trace element data are reported in Table S2. We analyzed a wide range of rock types from the BRO and so a wide range of trace element patterns are reported (Figure 3). Note that many ultramafic samples do not have sufficient trace element concentrations to be detected and therefore are not plotted here. Most samples have lower REE concentrations than N-MORB, regardless of rock type. Samples shown in Figure 3(a) have LREE/HREE > 1 or strong Eu anomalies. Samples in Figure 3(b) have LREE/HREE ≅ 1 or less. REE data from Harris [20] are also reported. Any gaps in the data indicate an element that was below the detection limit or not measured.

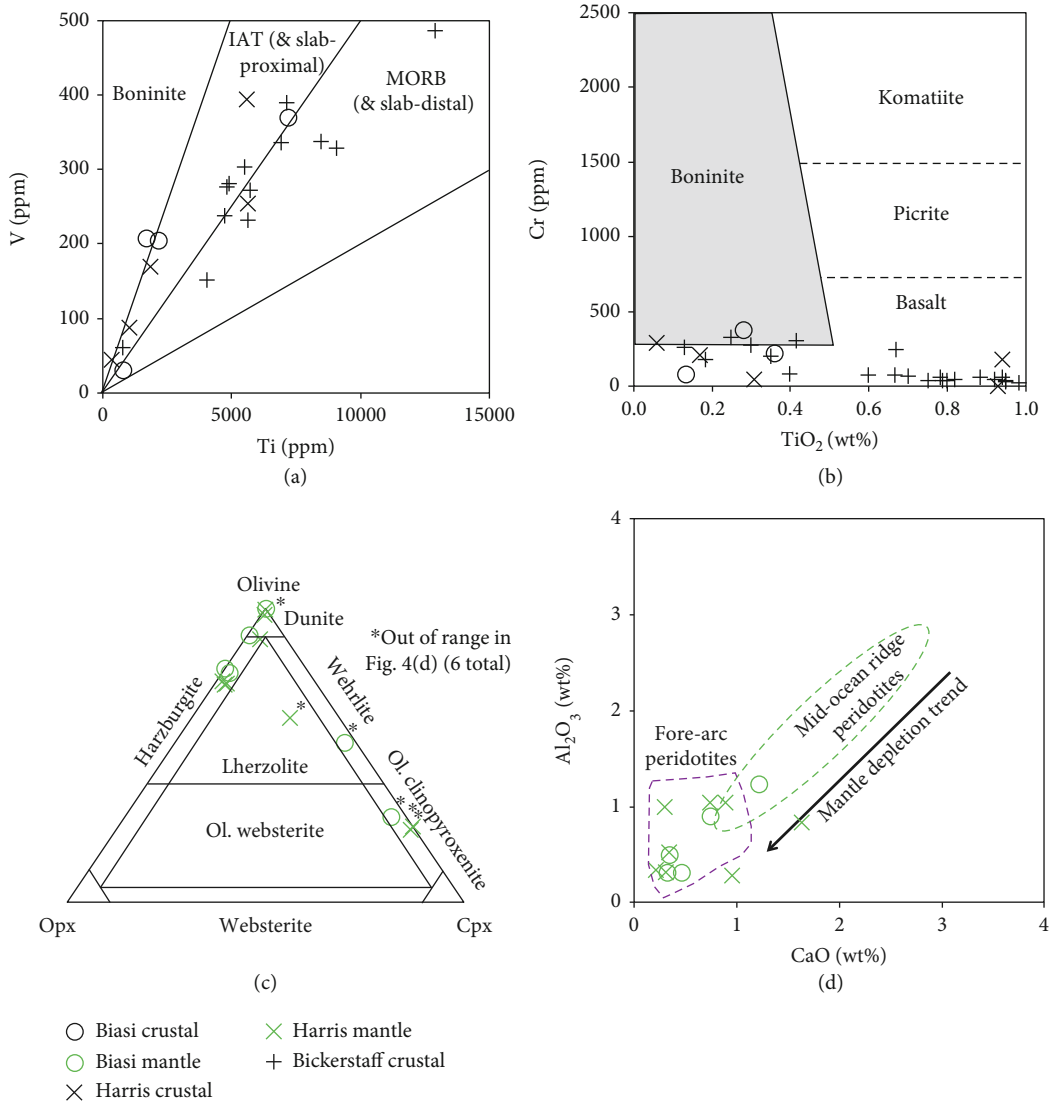

FIGURE 2: Major and trace element chemistry of the BRO. This is a compilation of new data (circles) and data from Harris [20] (×) and Bickerstaff [22] (+). (a, b) Only samples from the crustal section of the BRO, with <55 wt% SiO_2, and no obvious cumulate textures (layered gabbro, anorthosite, etc.) are shown. Note that many samples from Bickerstaff [22] do not have major-element analyses, and thus are not plotted here. (a) V vs. Ti diagram showing a range of affinities for BRO samples. Modified from Pearce [5] and Shervais [67]. (b) Boninite classification plot (immobile element version) showing boninitic compositions from some BRO crustal rocks. Modified from Pearce and Reagan [62]. (c) CIPW-normative mineralogy for BRO mantle samples. Modified from Coleman [68]. (d) BRO mantle samples have low Al_2O_3 and CaO, a common feature of forearc peridotites. Modified from Ishii et al. [69] and Gahlan et al. [70]. See text for discussion.

Samples in Figure 3(a) generally show negative REE slopes after N-MORB normalization. These consist mostly of plagioclase-bearing rocks. Samples with strong depletion of HREEs and positive Eu anomalies are probably plagioclase cumulates. This is certainly the case for sample 114 (anorthosite). The remaining samples in Figure 3(a) show smooth and monotonic REE patterns without prominent Eu anomalies. The three samples with LREE and LREE/HREE higher than MORB are plausibly liquid or near-liquid compositions derived from a source more enriched than the MORB source or by smaller degrees of melting than average N-MORB. The two hornblende gabbros with overall REE lower than MORB but LREE/HREE higher than MORB may be derived from similar liquids but likely contain abundant cumulate clinopyroxene that dilutes their overall REE concentrations.

Samples in Figure 3(b) show concave-down MORB-normalized REE patterns, with flat MREEs and small to significant depletion in LREE relative to N-MORB. The only volcanic sample of the series (117, sheeted dike) is part of this group, although it differs from the others in having MREE/HREE lower than MORB, whereas all the others have MREE/HREE greater than MORB. Note that the sheeted dike sample has similar REE concentrations to cumulates in the sample suite (pyroxenite, wehrlite, etc.), despite being a frozen liquid. The sheeted dike sample must be from a depleted source, a high degree of melting, or both.

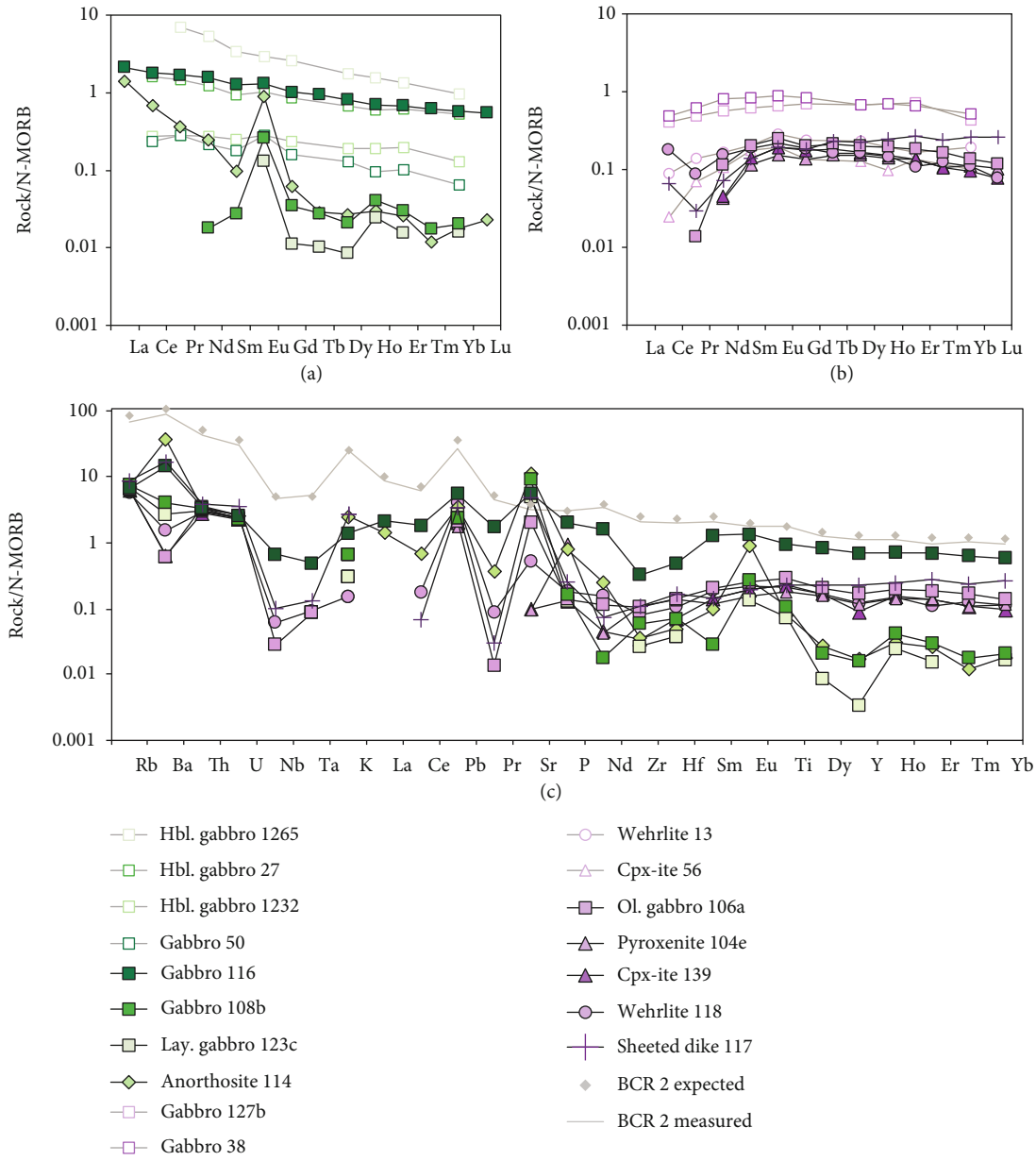

Figure 3: N-MORB-normalized trace element plots. Filled symbols are new data, and hollow symbols are data from Harris [20]. (a) Subset of BRO samples that show HREE depletion (or LREE enrichment). (b) BRO samples that show LREE depletion. (c) Extended trace element diagram. Only REE data exists for samples from Harris [20], so those samples are not plotted here. An example standard (BCR-2, run as an unknown) is shown in grey. "BCR Expected" values from the U.S. Geological Survey. See text for discussion. N-MORB normalizing values from Sun and McDonough [71].

Figure 3(c) shows additional N-MORB-normalized trace element abundances. Concentrations determined by ICP-MS are shown for all elements except for XRF determinations of K, P, and Ti. Notable features of the dataset include clear negative Nb-Ta anomalies, positive Pb anomalies, and highly variable Ba and Sr concentrations. A number of samples have negative Zr-Hf anomalies. The patterns clearly indicate a subduction influence in all of these samples [53], though the strength of the subduction signal varies.

Sample 117, the sheeted dike, shows positive anomalies in Ba, K, Pb, and Sr; strong negative Nb-Ta anomaly; and MORB-normalized levels of Pr, Ce, and P similar to the HREEs. These signatures have all been associated with a subduction influence derived from a slab at relatively shallow levels (see Figure 4 in Pearce and Stern [53]). In contrast, sample 116 (gabbro) shows weaker subduction-input signals, despite being more enriched overall. This sample also shows higher levels of Pr, Ce, and P, compared to HREEs, suggesting a mostly deep subduction component [53]. Its high concentrations of incompatible elements and smooth overall pattern indicates that 116 can be interpreted as a frozen liquid. The extended trace element pattern of sample 114 (anorthosite), with elevated Ba, confirms plagioclase accumulation in this sample. Other samples (106a, 104e, 118, and 139)

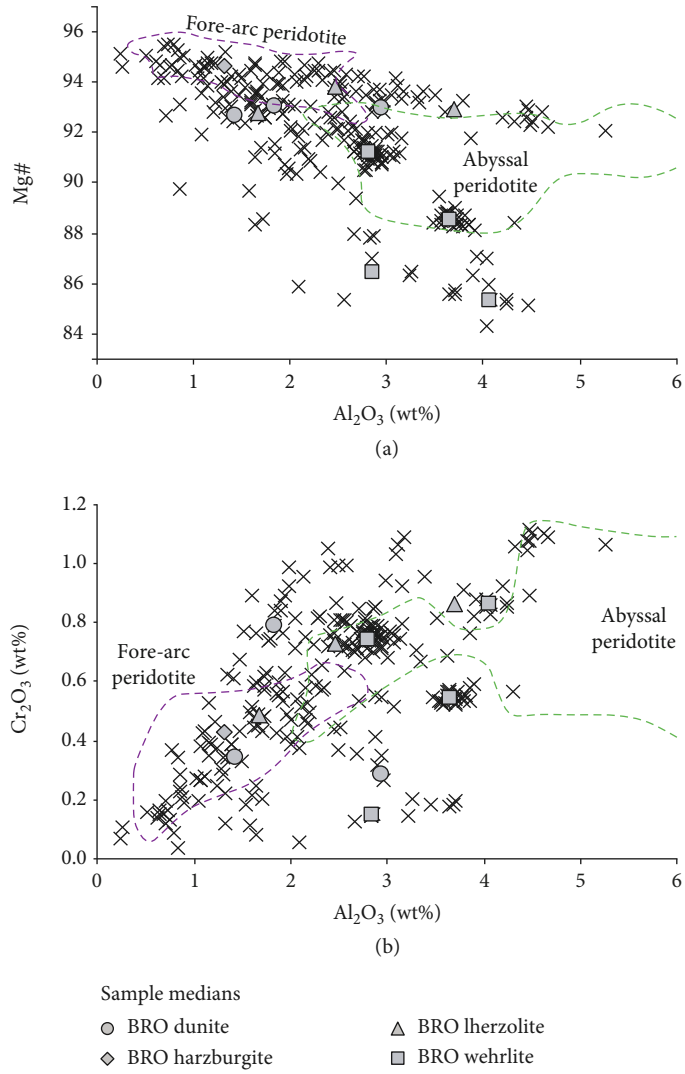

FIGURE 4: Clinopyroxene mineral chemistry of representative BRO mantle samples. Individual analyses are shown with "×" symbols. Fields based on Pagé et al. [55]. See text for discussion.

show negative Ba anomalies; these are olivine-clinopyroxene cumulates that left Ba in the residual liquid. Finally, two likely cumulate samples, 108b and 123c, presumably reflect a combination of plagioclase and mafic mineral accumulation.

Trace element data and petrography therefore indicate that two samples (sheeted dike 117 and gabbro 116) are likely frozen liquids whereas most other samples are (at least partially) cumulates. Of the frozen liquids, 117 shows evidence of a high extent of melting and a significant shallow subduction signal, while 116 shows evidence of a small degree of melting or enriched source and some deep subduction input. All remaining samples show some subduction signatures as well but are more difficult to interpret due to crystal accumulation. Finally, based on overlapping REE patterns, it is likely that the Harris [20] samples also include a mixture of frozen liquids and cumulates. Harris [20] did not report extended trace element data so this cannot be confirmed.

4.4. Mineral Chemistry. SEM/EDS compositional mapping shows that mantle rocks of the BRO contain olivine, chromite, clinopyroxene, orthopyroxene, and (in some samples) minor plagioclase. Large chromitite layers that include economically viable abundances of platinum group elements can be found in the mantle section of the BRO [54]. In the gabbro and crustal rocks, plagioclase, clinopyroxene, minor orthopyroxene, minor amphibole, and minor olivine are present. Minor amounts of euhedral apatite are also present in some of the gabbro samples. See Table S1 for a partial list of the observed phases in each sample.

Mineral data collected via EMP are shown in Figures 4, 5, 6, and 7. Clinopyroxene data from BRO mantle samples are shown in Figure 4. There is considerable scatter in the data, probably due to a combination of fractional crystallization, partial melting, and other processes. This likely explains why several samples fall outside the fields of Pagé et al. [55]. Regardless, the data generally shows a mixture of fore-arc and abyssal affinities.

Spinel data from a variety of peridotites representing various tectonic settings are shown in Figure 5. BRO spinel compositions vary widely, whereas most tectonic localities show

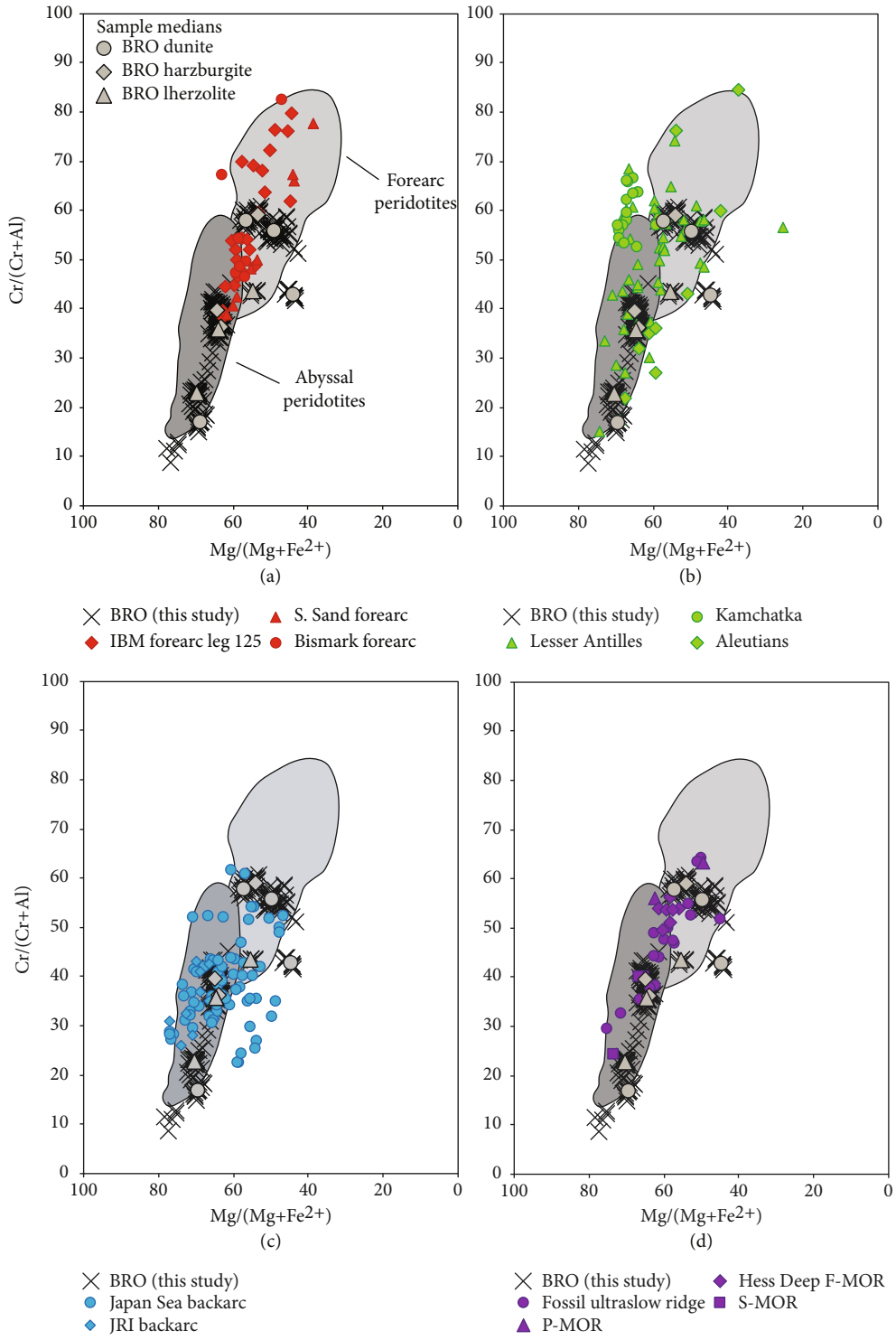

Figure 5: Cr-spinel data from BRO mantle lithologies (Table S6) and a compilation of data from multiple tectonic settings. Compiled data is sourced from peridotite xenoliths and exposures of mantle peridotites. BRO data is shown with black "×" symbols, and BRO sample median values are shown with grey symbols. (a) Comparison of BRO data (this study) with spinel from forearc settings. Data from Pearce et al. [56], Parkinson and Pearce [58], McInnes et al. [59], and Gregoire et al. [72]. (b) Compilation of spinel data from arcs. Data from Ionov [73], Parkinson et al. [74], Vannucci et al. [75], Conrad and Kay [76], and Debari et al. [77]. (c) Comparison with back-arc spinel. JRI = James Ross Island, Antarctica. Data from Calabozo et al. [78], Altunkaynak et al. [79], and Ichiyama et al. [80]. (d) Comparison with midocean ridge (MOR) spinel data. P = slow-spreading plume related; S = slow-spreading ridge; F = fast-spreading ridge. Data from Sanfilippo et al. [81] and Dare et al. [82]. Modified from Arai and Ishimaru [83].

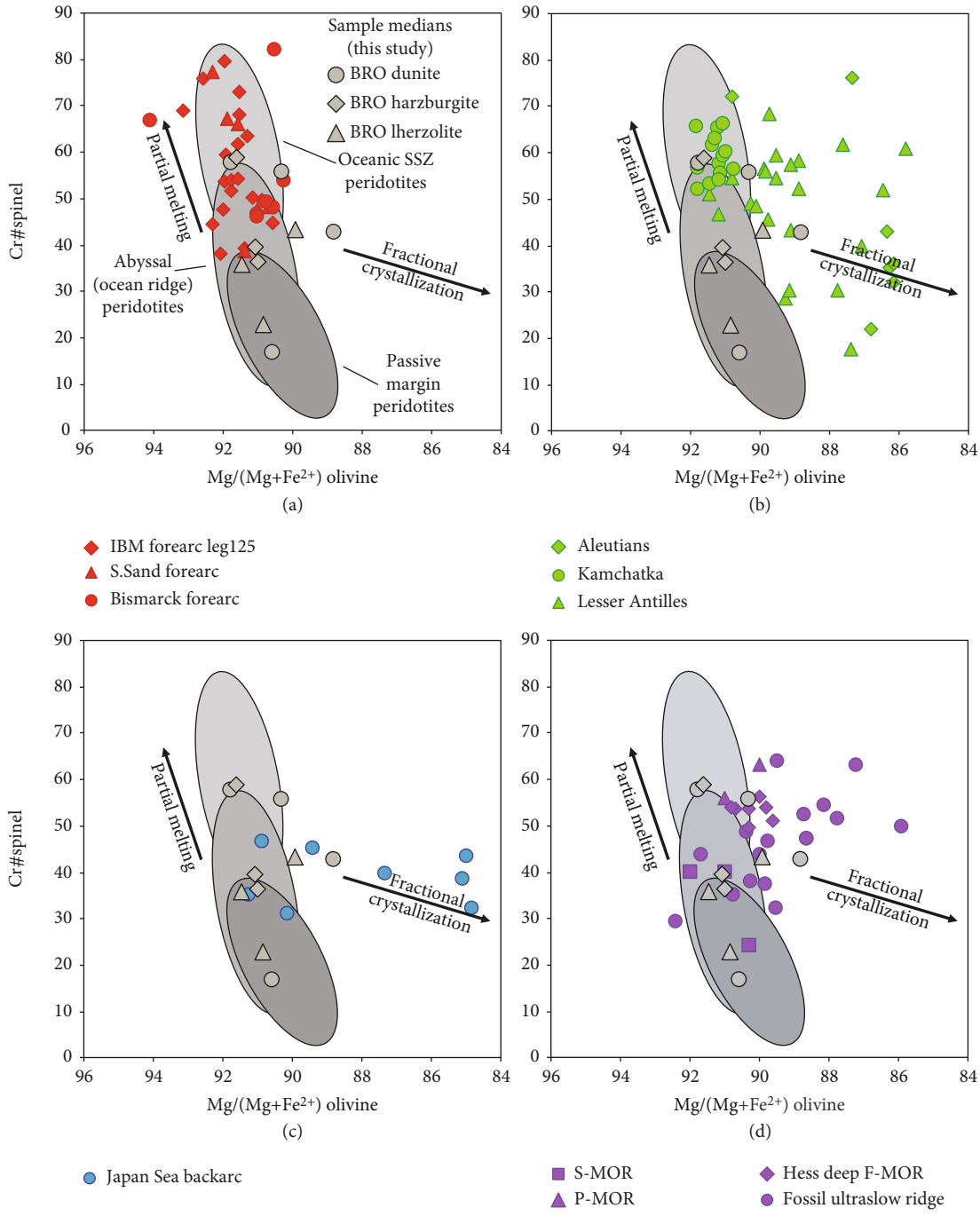

Figure 6: Cr-spinel and olivine data from BRO mantle lithologies (Tables S3, S4, and S6) and a compilation of data from various settings. Plotted on discrimination diagram of Pearce et al. [56]. Data sources and symbols as in Figure 5. See text for discussion.

more tightly clustered spinel compositions; only peridotite from oceanic arc settings show such a large range in a single locality (Figure 5(b); Aleutians, Lesser Antilles). Nevertheless, the overlap in spinel composition between the BRO and other settings (midocean ridges, forearcs, and back-arcs) makes it difficult to exclude any of these settings based on spinel compositions alone.

Combined spinel-olivine data is shown in Figure 6. BRO samples with high spinel Cr# are similar to samples from forearc and arc settings (Figures 6(a) and 6(b)). Midocean ridge data also overlaps with some of the BRO data. BRO samples with low spinel Cr# do not significantly overlap with any of the tectonic settings presented here. These samples plot within the passive margin/abyssal peridotite field of Pearce et al. [56]. Some BRO samples plot outside the olivine-spinel mantle array, likely indicating that melt-rock reaction, fractional crystallization, or low-temperature reequilibration may have lowered the Mg# of olivine and spinel

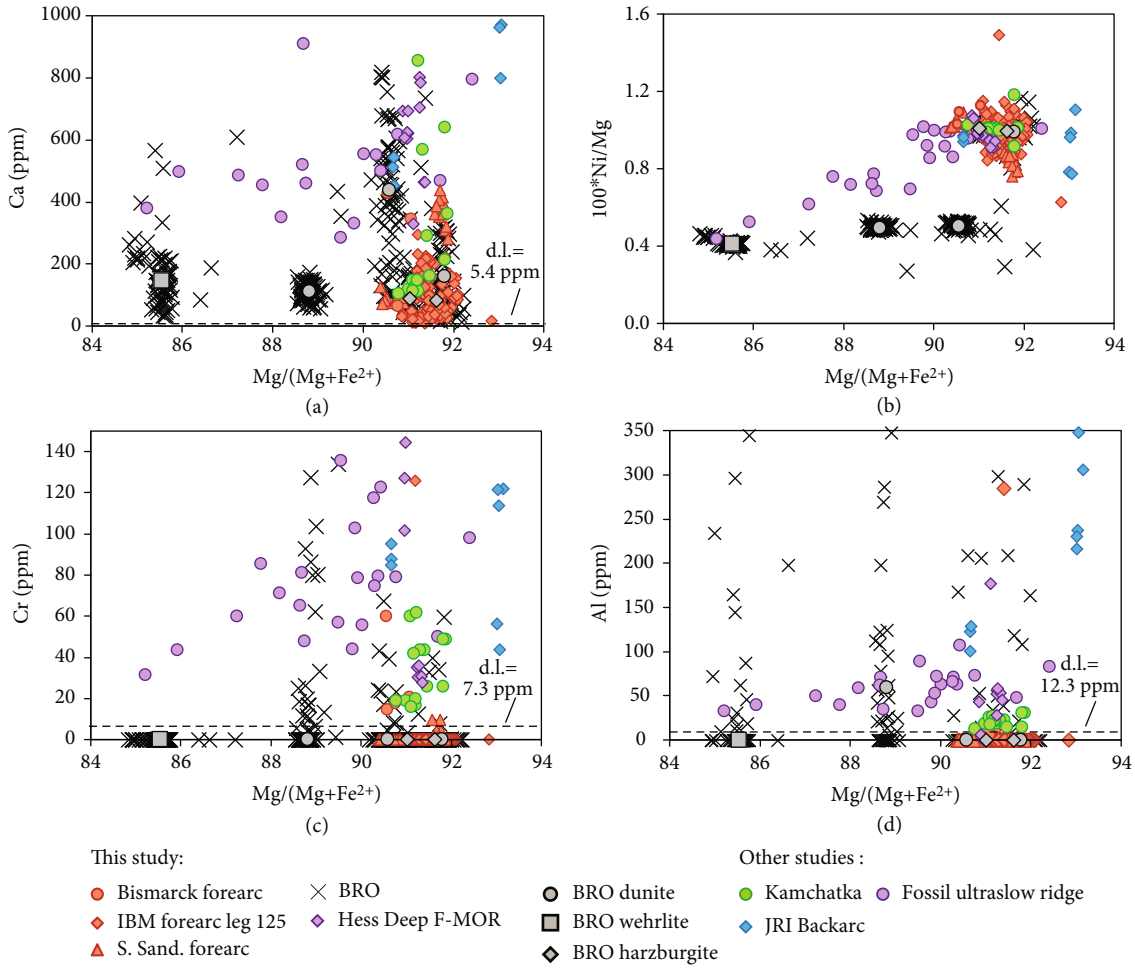

FIGURE 7: High-precision olivine analyses from BRO mantle lithologies (Table S4) and a compilation of data from various tectonic settings. Grey symbols are median values for BRO samples. Analyses with no detectable signal are plotted on the *x*-axis. Data from the BRO, IBM forearc Leg 125, S. Sandwich forearc, and Hess Deep are from this study. Other analyses are from Gregoire et al. [72], Ionov [73], Altunkaynak et al. [79], and Sanfilippo et al. [81]. Leg 125 samples are harzburgites from Conical and Torishima Seamounts in the IBM forearc. Hess Deep samples are harzburgites from ODP Leg 147 (site 895). Scotia samples are harbzurgites from the South Sandwich forearc. d.l. = detection limit. See Dare et al. [82] and Pearce et al. [56] for more sample details. See text for discussion.

in these samples [57]. One dunite outlier has particularly low Cr# spinel. This sample is very spinel-rich and has a more complex origin than can be adequately captured by the plot.

High-current olivine data are presented in Figure 7. These analyses make use of high EMP beam currents and long counting times to lower detection limits of trace elements (Al, Co, and Cr) and improve precision of minor elements (Ca, Mn, and Ni) in olivine. Fewer data from the literature are available due to the relative rarity of high-precision olivine analyses. Data for olivine from the BRO, Izu-Bonin forearc (Leg 125), South Sandwich forearc, and Hess Deep were gathered in this study. Other data in Figure 7 are compiled from the literature (see figure caption). The four plots in Figure 7 were chosen because, among chemical signatures in olivine, these elements offer the best discrimination among tectonic settings. Figures 7(a) and 7(b) show that olivine in the BRO harzburgite samples and in one dunite overlaps with arc/forearc data. Olivine from the BRO wehrlite sample and the other two dunite samples differs in at least one of the plotted elements from olivine in peridotites from any other tectonic setting. These samples evidently have anomalous histories of fractionation or melt-rock reaction that make them inappropriate for comparison to residual peridotites. BRO olivine, especially from the harzburgite and the "normal" dunite, has notably low Cr and Al (Table S4). This distinct feature is shared by other forearc samples in this study (Figures 7(c) and 7(d)) and is, based on the available data, a feature uniquely associated with forearc peridotite. All other samples, including Hess Deep samples analyzed in this study, show higher levels of Cr and Al. This may be explained by high degrees of melt extraction and the persistent presence of residual chromium-spinel. High Cr# spinel is a prominent accessory phase in mantle rocks of the BRO, IBM forearc, S. Sandwich forearc, and Bismarck forearc [56, 58, 59]. Low Ca-contents might be best explained by elevated magmatic water in the subduction-influenced system compared to the MORB system; water activity acts to decrease the partition

coefficient for Ca in olivine and promote efficient Ca extraction from these residual rocks [60].

5. Discussion

5.1. Tectonic Setting. Previous studies of the BRO have concluded that it was created in an SSZ environment [7, 20]. The data presented above clearly supports this conclusion. Other tectonic environments such as midocean ridges can be immediately ruled out based on the arc-like trace element patterns (Figure 3), whole-rock data from both the crust and mantle sections of the BRO (Figures 2(a) and 2(d)), and the high-precision olivine data (Figures 7(c) and 7(d)). The assignment of the BRO to an SSZ setting has very high confidence.

Distinguishing between different SSZ settings is more difficult. Arc, forearc, and back-arc geochemical signatures often overlap. Notably, arc settings with complex tectonic histories can have signatures of multiple SSZ environments in cotemporal rocks (e.g., [61]). This is likely due to inheritance of geochemical signals from previous tectonic settings in the same area.

Nevertheless, the available geochemical data suggests that the BRO was created in a forearc setting. High-precision olivine analyses from the BRO uniquely overlap with forearc peridotites (Figure 7). Whole-rock data from the mantle section of the BRO also show a predominantly forearc signature (Figure 2(d)). Much of the spinel and olivine chemistry (Figures 5 and 6) also agrees with a forearc setting. However, some whole-rock and mineral compositions lie outside the known range of forearc samples (Figures 2(d), 4, 6(b), and 7). These data are from complex plutonic rocks with possible histories of crystal accumulation, melt-rock reaction, or late reequilibration. They do not consistently match residual or volcanic samples from any other tectonic setting either. These samples reveal the hazards of working with intrusive crustal samples and atypical mantle samples; they would likely have been excluded from a study of a more accessible and better-sampled locality. Given the small total number of samples available from the BRO, we analyzed these samples anyway and it is remarkable that the tectonic setting is evident in our overall dataset despite the complexity of these rocks. Given the strong subduction signals in the trace element data (Figure 3), we cannot rule out a history of arc or back-arc influence on the mantle samples that later become incorporated in the BRO. Another possibility is that the forearc setting of the BRO gradually evolved into an oceanic arc setting prior to obduction of the ophiolite.

5.2. Possible Subduction Initiation. The only extrusive sample in the new dataset, 117 (sheeted dike), has a boninitic composition (Figure 2(d), Table S2a). In the Phanerozoic, boninites are found predominantly in subduction-initiation (SI) settings, but have been found in intraplate settings as well [62]. As outlined by previous authors [4, 63], an SI setting can be identified by a temporal evolution from initially MORB-like lavas to boninites to arc-like lavas. The BRO lacks a sufficiently thick and stratigraphically coherent extrusive section to make this identification. The trace element composition of the sheeted dike (117) has a signature of a shallow subduction component (Figure 3(c)). This is a characteristic feature of trench-proximal magmas, while deeper subduction signals are found in magmas farther from the trench (arc and back-arc) [53]. The combination of a boninitic composition and a shallow subduction component make it difficult to argue for any tectonic origin for 117 other than subduction initiation. Other samples have boninitic compositions, but we do not have accompanying trace element data for these samples. However, a small number of boninitic samples are not diagnostic of the entire ophiolite, and more samples are needed to make a definitive case for subduction initiation. Another sample, 116 (gabbro), is likely a frozen liquid that preserves both deep and shallow subduction signatures. This is not unusual, given the mix of forearc and other arc signals seen in the mineral and whole-rock chemistry of the BRO. Conceivably, sample 116 represents a later stage than sample 117 in the evolution of the subduction system.

Based on the geochemical data presented here, we conclude that the BRO was created in a forearc setting. Although there is some suggestion from the data that the BRO preserves a subduction-initiation event, we cannot definitively rule out other formation scenarios such as slab rollback. Other geologic evidence that has already been collected on the BRO is consistent with either origin for these rocks and does not greatly affect the subsequent tectonic history (see below).

5.3. Genesis of the BRO

5.3.1. Existing Tectonic Constraints. The new data presented here suggest that the BRO formed in a forearc setting. This interpretation is in agreement with previous work that classified the BRO as a suprasubduction zone ophiolite [7, 20]. The earlier classification was not precise enough to delineate between different suprasubduction zone settings for the BRO. Its new classification as a forearc ophiolite allows us to tie in the BRO's genesis with specific tectonic events.

The tectonic history of northern/interior Alaska is poorly constrained. This is partly due to difficult access and lack of exposure. Any tectonic history will inevitably involve simplifications of existing constraints. For the tectonic history of the BRO, the following are the most important constraints from various studies:

(1) This study yields several lines of geochemical evidence documenting that the BRO formed in a forearc setting. A zircon age of 170 ± 3 Ma was determined from a late-stage plagiogranite in the BRO [26] and likely represents a minimum age for the BRO. Overlapping $^{40}Ar/^{39}Ar$ ages from BRO gabbro and the metamorphic sole [7], together with documented amphibolite facies metamorphism and partial melting of the sole [21], suggest that the BRO was still young and hot during emplacement at ~165 Ma

(2) Sparse geochronological data exists for the Koyukuk Arc (currently to the south of the BRO). On the basis of invertebrate fossils and K-Ar ages [15] from

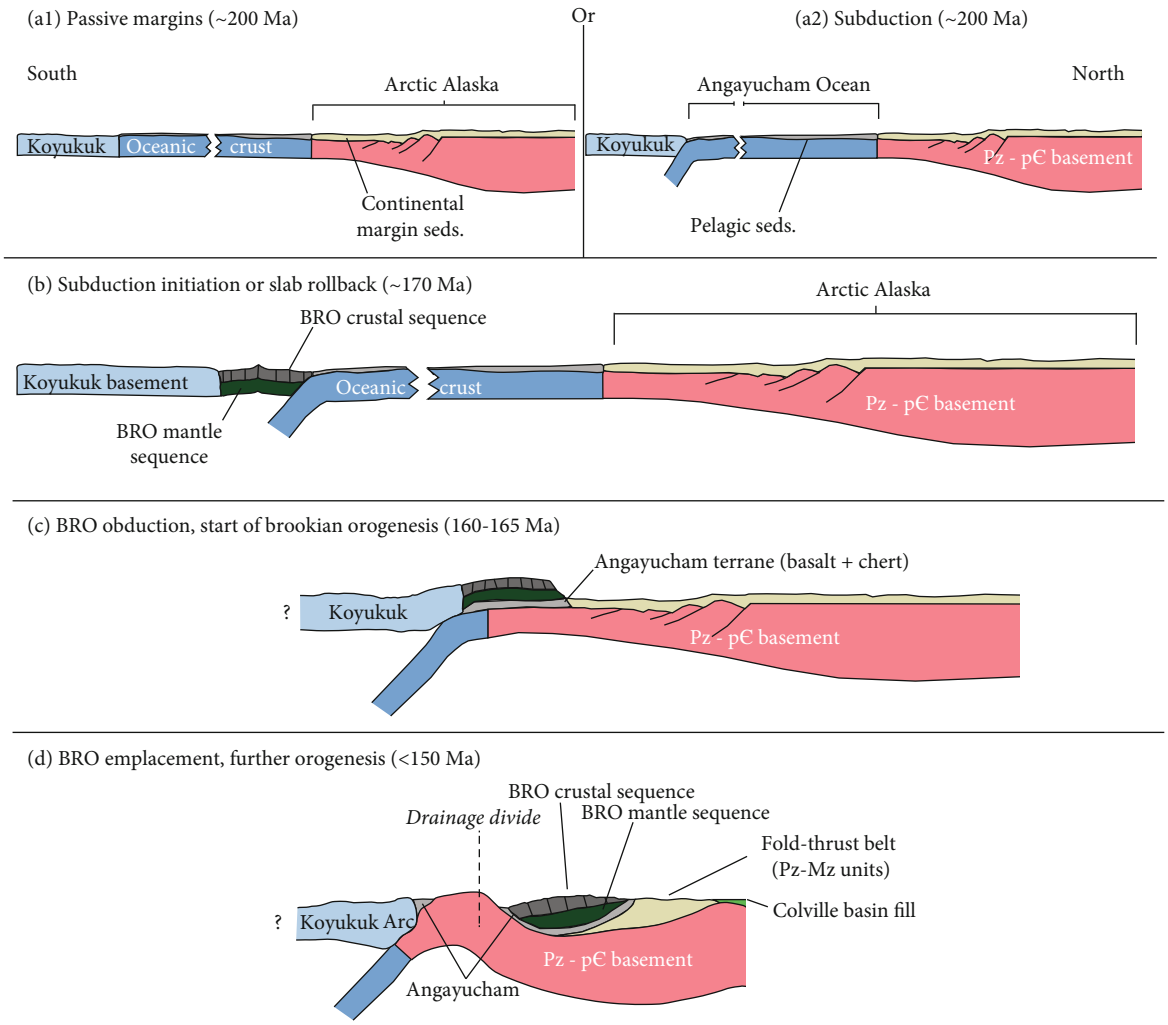

FIGURE 8: Genesis and emplacement of the BRO. Two initial conditions are possible, depending on whether the BRO was formed via subduction initiation or slab rollback. (a1) Both the Arctic Alaska and Koyukuk margins are passive, or (a2) a subduction zone already exists along northern margin of the Koyukuk terrane (present-day coordinates). (a1, a2) A sea of unknown size (shown by a break in the section) separates the Arctic Alaska passive margin from the oldest units of the Koyukuk terrane [15]. (b) Either southward subduction or slab rollback begins at the northern Koyukuk margin. The BRO is created in the Koyukuk forearc during this event. (c) Collision between the Koyukuk terrane and the continental margin causes the BRO to obduct over Angayucham basalts/sediments and onto Arctic Alaska [40]. (d) Further orogenesis separates the BRO from the Koyukuk Arc [7, 65].

igneous samples, the arc was active in the early-middle Jurassic. Voluminous felsic magmatism began around 150 Ma in the arc [15, 45]; the timing and extent of magmatism prior to this is not well constrained

(3) The lowermost units of the Brookian foreland (Colville) basin contain abundant BRO-age clasts and detrital zircons, suggesting that these units were partially sourced from the BRO [23].

(4) The lowermost exposed units of the Yukon-Koyukuk basin (YKB) contain comparatively few BRO-age detrital zircons. Instead, they contain abundant mafic clasts that mostly predate the BRO (early Jurassic to Triassic). This is interpreted as evidence for an arc terrane in this area during this time [49].

5.3.2. Mafic Detritus, Relation to the BRO. A recent detrital zircon study of 112 Ma and younger units in the NW corner of the Yukon-Koyukuk basin (YKB, Figure 1) found abundant mafic detritus and cobbles in the lowermost exposed sedimentary units (Type 1 of O'Brien et al. [49]). These sediments have an arc-like signature and a prominent population of 160-240 Ma detrital zircons with juvenile εHf signatures. In addition, the sediments have abundant detrital Cr-spinel, some of which shows a forearc signature. This led O'Brien et al. [49] to conclude that a Triassic-Jurassic juvenile arc terrane must have supplied this mafic-ultramafic material to the YKB. They further conclude that the Angayucham terrane (including the BRO) is the modern remnant of this arc. Finally, they exclude the Koyukuk Arc as a possible source of these sediments, due to a lack of exposed lithologies of the appropriate age.

While this interpretation is consistent with their data, it is not consistent with other geologic evidence from the BRO and Angayucham terrane. The eroding BRO was cut off from the YKB by a drainage divide at >113 Ma, and instead eroded into the Colville basin [23, 49]. Although the BRO's minimum age of 165-170 Ma is within the range of detrital zircons found by O'Brien et al. [49], the ophiolite was still young and hot during emplacement [7]. Therefore, the ophiolite cannot account for most of the detrital zircon ages within the 160-240 Ma population of interest. The structurally underlying Angayucham terrane is not an arc either. Basalts from this terrane (where it is exposed in the Brooks Range) primarily have an oceanic plateau/MORB affinity [17, 21, 28, 29]. Given the >50 m.y. gap between the depositional age of the unit samples by O'Brien et al. [49] and the age of the 160-240 Ma detrital zircons, it is very difficult to determine where the zircons originally crystallized. It is possible that mafic detritus in the YKB was derived locally from somewhere in interior Alaska. For example, there is relatively little geochemical or geochronological data on areas mapped as Angayucham terrane outside of the Brooks Range (in interior Alaska); some of these may preserve an early Mesozoic arc. It is possible that, with more geochronological data from the BRO, material suitable to be the source of YKB sediments could be found. At the moment, however, more data are needed from possible source areas to determine the provenance of these sediments.

5.3.3. Onset of Brookian Orogenesis. Our model of genesis and emplacement of the BRO is illustrated in Figure 8. In the middle Jurassic, the only arc-related terranes in this area were the BRO and the Koyukuk Arc [7, 35]. Given the BRO's forearc setting, it is most likely the preserved remnant of the Koyukuk forearc. This puts the BRO in-between the Koyukuk Arc and the Arctic Alaska continental margin (Figure 8(b)). The first part of the distal continental margin to encounter the BRO is the Angayucham terrane. The lithologies within the BRO metamorphic sole and underlying unmetamorphosed units match those in the Angayucham terrane and distal parts of the Etivluk group of the Arctic Alaska passive margin [21]. The youngest passive margin units overlap in age (~163-169 Ma, [7]) with ophiolite cooling and emplacement [39]. These lithologic and age relations constrain the onset age of age Koyukuk-Arctic Alaska collision (Brookian orogeny) to obduction of BRO (Figure 8(c)).

Several authors have linked the onset of Brookian orogenesis and blueschist-facies metamorphism in the region to a collision between the Koyukuk Arc and Arctic Alaska [32, 39, 44, 64]. As discussed earlier, this event has been very difficult to date, due to greenschist overprinting of the original blueschist-facies metamorphism. However, collisional deformation and metamorphism of the Arctic Alaska passive margin must coincide with obduction of the BRO (Figures 8(b) and 8(c)). Therefore, we can conclude that Brookian orogenesis began around 169 Ma, which is the maximum age of BRO obduction [7]. Later extension in the Brooks Range would separate the BRO from the Koyukuk Arc (Figure 8(d); Harris et al. [7]; Law et al. [65]). This separation is consistent with different detrital zircon populations seen in mafic material from the Brookian foreland and YKB [23, 49].

The tectonic history outlined above and in Figure 8 is a hybrid between several previously proposed models. However, it is consistent with the published detrital zircon record of surrounding basins, the BRO geochemistry and geochronology, and the geochronology of the Koyukuk Arc. Furthermore, it provides an upper age limit for the timing of blueschist metamorphism in the area [45, 64] and provides a well-constrained age of 163-169 Ma for the onset of Brookian orogenesis.

6. Conclusions

New geochemical data presented in this study shows that the Brooks Range ophiolite formed in a forearc setting. Some of this data suggests that subduction initiation played a role in the formation of the BRO, but more evidence is needed to support this hypothesis. It is likely that the BRO inherited some arc-like geochemical signatures from the neighboring Koyukuk Arc or evolved to a more mature subduction state before obduction. The BRO's proximity to distal Arctic Alaska passive margin at the time it formed and was obducted (~169 Ma) constrains the onset of the Brookian orogen.

Data Availability

Supplemental Tables S1–S6, which contain all of the new geochemical data used in this study, are available with the online version of this article.

Disclosure

Portions of this work were presented at the American Geophysical Union 2017 meeting under a similar title: "T23C-0619: Tectonochemistry of the Brooks Range Ophiolite, Alaska."

Conflicts of Interest

The authors are not aware of any financial conflicts or any other conflicts of interest that would affect the content of this study.

Acknowledgments

The authors of this study wish to thank Mike Dorais, Tober Dyorich, Chi Ma, and Nathan Dalleska for assistance with laboratory analyses. Betsy Friedlander, Lyle Nelson, and Teck Resources are greatly thanked for obtaining Iyokrok samples. We are grateful to Julian Pearce for sharing the IBM, South Sandwich, and Hess Deep thin sections. This work is supported in part by the United States National Science Foundation, award EAR-1550934.

Supplementary Materials

Supplemental Tables S1–S6, which contain all of the new geochemical data used in this study, are available with the online version of this article. *(Supplementary Materials)*

References

[1] J. Wakabayashi and Y. Dilek, "What constitutes "emplacement" of an ophiolite?: mechanisms and relationship to subduction initiation and formation of metamorphic soles," *Geological Society, London, Special Publications*, vol. 218, no. 1, pp. 427–447, 2003.

[2] J. A. Pearce, M. Reagan, K. Petronotis et al., "International Ocean Discovery Program. Expedition 352 Preliminary Report. Izu-Bonin-Mariana fore arc: testing subduction initiation and ophiolite models by drilling the outer Izu-Bonin-Mariana fore arc; 30 July-29 September 2014," *Preliminary Reports (International Ocean Discovery Program)*, vol. 352, pp. 1–86, 2015.

[3] M. K. Reagan, J. A. Pearce, K. Petronotis et al., "Subduction initiation and ophiolite crust: new insights from IODP drilling," *International Geology Review*, vol. 59, no. 11, pp. 1439–1450, 2017.

[4] S. A. Whattam and R. J. Stern, "The "subduction initiation rule": a key for linking ophiolites, intra-oceanic forearcs, and subduction initiation," *Contributions to Mineralogy and Petrology*, vol. 162, no. 5, pp. 1031–1045, 2011.

[5] J. A. Pearce, "Immobile element fingerprinting of ophiolites," *Elements*, vol. 10, no. 2, pp. 101–108, 2014.

[6] M. K. Reagan, O. Ishizuka, R. J. Stern et al., "Fore-arc basalts and subduction initiation in the Izu-Bonin-Mariana system," *Geochemistry, Geophysics, Geosystems*, vol. 11, no. 3, 2010.

[7] R. Harris, "Tectonic evolution of the Brooks Range ophiolite, northern Alaska," *Tectonophysics*, vol. 392, no. 1-4, pp. 143–163, 2004.

[8] A. Martin, "Structure and tectonic history of the Western Brooks Range, De Long Mountains and Lisburne Hills, Northern Alaska," *Geological Society of America Bulletin*, vol. 81, no. 12, pp. 3605–3622, 1970.

[9] I. Tailleur, "Structure and stratigraphy of Western Arctic Alaska. Abstract," *AAPG Bulletin*, vol. 54, pp. 2508–2508, 1970.

[10] D. Roeder and C. G. Mull, "Tectonics of Brooks Range ophiolites, Alaska: geologic notes," *AAPG Bulletin*, vol. 62, pp. 1696–1702, 1978.

[11] M. Churkin, W. J. Nokleberg, and C. Huie, "Collision-deformed Paleozoic continental margin, western Brooks Range, Alaska," *Geology*, vol. 7, no. 8, pp. 379–383, 1979.

[12] W. Gealey, "Ophiolite obduction mechanism," *Proceedings of the Ophiolites: Proceedings of the International Ophiolite Symposium, Nicosia*, , pp. 228–243, Cyprus Geological Survey Department, 1980.

[13] E. Moores, "Origin and emplacement of ophiolites," *Reviews of Geophysics*, vol. 20, no. 4, pp. 735–760, 1982.

[14] C. F. Mayfield, I. L. Tailleur, I. Ellersieck, and G. Gryc, "Stratigraphy, structure, and palinspastic synthesis of the western Brooks Range, northwestern Alaska," *US Geological Survey Professional Paper*, vol. 1399, pp. 143–186, 1988.

[15] S. E. Box and W. W. Patton, "Igneous history of the Koyukuk Terrane, western Alaska: constraints on the origin, evolution, and ultimate collision of an accreted island arc terrane," *Journal of Geophysical Research: Solid Earth*, vol. 94, no. B11, pp. 15843–15867, 1989.

[16] E. L. Miller and T. L. Hudson, "Mid-Cretaceous extensional fragmentation of a Jurassic-Early Cretaceous compressional orogen Alaska," *Tectonics*, vol. 10, no. 4, pp. 781–796, 1991.

[17] S. M. Karl, *Arc and extensional basin geochemical and tectonic affinities for Maiyumerak basalts in the western Brooks Range*, Geologic studies in Alaska by the U.S. Geological Survey, 1990.

[18] K. R. Wirth and J. M. Bird, "Chronology of ophiolite crystallization, detachment, and deeper parts of subduction zones. Emplacement: evidence from the Brooks Range, Alaska," *Geology*, vol. 20, no. 1, pp. 75–78, 1992.

[19] R. Harris, "Peri-collisional extension and the formation of Oman-type ophiolites in the Banda Arc and Brooks Range," *Geological Society, London, Special Publications*, vol. 60, no. 1, pp. 301–325, 1992.

[20] R. Harris, "Geochemistry and tectonomagmatic affinity of the Misheguk massif, Brooks Range ophiolite, Alaska," *Lithos*, vol. 35, no. 1-2, pp. 1–25, 1995.

[21] R. Harris, "Origin and tectonic evolution of the metamorphic sole beneath the Brooks Range ophiolite, Alaska," *Special Papers-Geological Society of America*, pp. 293–312, 1998.

[22] D. Bickerstaff, *The crustal section of the Siniktanneyak Mountain ophiolite, Brooks Range, Alaska*, West Virginia University, Morgantown, WV, 1994.

[23] T. E. Moore, P. B. O'Sullivan, C. J. Potter, and R. A. Donelick, "Provenance and detrital zircon geochronologic evolution of lower Brookian foreland basin deposits of the western Brooks Range, Alaska, and implications for early Brookian tectonism," *Geosphere*, vol. 11, no. 1, pp. 93–122, 2015.

[24] K. R. Wirth, *Processes of lithosphere evolution: Geochemistry and tectonics of mafic rocks in the Brooks Range and Yukon-Tanana Region, Alaska*, Ph.D., Cornell University, Ithaca, NY, 1991.

[25] K. R. Wirth, J. M. Bird, A. E. Blythe, D. J. Harding, and M. T. Heizler, "Age and evolution of western Brooks Range ophiolites, Alaska: results from $^{40}Ar/^{39}Ar$ thermochronometry," *Tectonics*, vol. 12, no. 2, pp. 410–432, 1993.

[26] T. E. Moore, J. N. Aleinikoff, and M. Walter, "Middle Jurassic U-Pb crystallization age for Siniktanneyak Mountain ophiolite, Brooks Range, Alaska," *Geological Society of America, Abstracts with Programs;(United States)*, vol. 25, 1993.

[27] N. J. Silberling, D. Jones, J. W. H. Monger, P. Coney, H. C. Berg, and G. Plafker, *Lithotectonic terrane map of Alaska and adjacent parts of Canada*, 1994.

[28] F. Barker, D. L. Jones, J. R. Budahn, and P. J. Coney, "Ocean plateau-seamount origin of basaltic rocks, Angayucham terrane, central Alaska," *The Journal of Geology*, vol. 96, no. 3, pp. 368–374, 1988.

[29] J. S. Pallister, J. R. Budahn, and B. L. Murchey, "Pillow basalts of the Angayucham terrane: oceanic plateau and island crust accreted to the Brooks Range," *Journal of Geophysical Research: Solid Earth*, vol. 94, no. B11, pp. 15901–15923, 1989.

[30] W. W. Patton Jr., S. E. Box, D. J. Grybeck, G. Plafker, and H. C. Berg, "Ophiolites and other mafic-ultramafic complexes in Alaska," in *The Geology of Alaska*, Geological Society of America, 1994, ISBN 978-0-8137-5453-6.

[31] V. Pease, "Chapter 20. Eurasian orogens and Arctic tectonics: an overview," *Geological Society, London, Memoirs*, vol. 35, no. 1, pp. 311–324, 2011.

[32] G. E. Shephard, R. D. Müller, and M. Seton, "The tectonic evolution of the Arctic since Pangea breakup: integrating constraints from surface geology and geophysics with mantle structure," *Earth-Science Reviews*, vol. 124, pp. 148–183, 2013.

[33] V. Pease, S. Drachev, R. Stephenson, and X. Zhang, "Arctic lithosphere—a review," *Tectonophysics*, vol. 628, pp. 1–25, 2014.

[34] J. M. Amato, J. Toro, V. V. Akinin, B. A. Hampton, A. S. Salnikov, and M. I. Tuchkova, "Tectonic evolution of the Mesozoic South Anyui suture zone, eastern Russia: a critical component of paleogeographic reconstructions of the Arctic region," *Geosphere*, vol. 11, no. 5, pp. 1530–1564, 2015.

[35] A. B. Till, "A synthesis of Jurassic and Early Cretaceous crustal evolution along the southern margin of the Arctic Alaska-Chukotka microplate and implications for defining tectonic boundaries active during opening of Arctic Ocean basins," *Lithosphere*, vol. 8, no. 3, pp. 219–237, 2016.

[36] N. Kuznetsov, "The Cambrian Baltica-Arctida collision, pre-Uralide-Timanide orogen, and its erosion products in the Arctic," in *Doklady Earth Sciences; Vol. 411*, pp. 1375–1380, Springer, 2006.

[37] J. Dumoulin, A. Till, and D. Bradley, "Neoproterozoic-Paleozoic paleogeographic reconstruction of the Arctic Alaska-Chukotka terrane," *Stone, DB, Clough, JG, and Thurston, DK, compilers, Geophysical Institute Report UAG*, 2011.

[38] D. Jones, N. J. Silberling, P. Coney, and G. Plafker, "Lithotectonic terrane map of Alaska (west of the 141st meridian)," *USGS Miscellaneous Field Studies Map*, vol. 1, 1987.

[39] T. E. Moore, W. K. Wallace, K. J. Bird, S. M. Karl, C. G. Mull, and J. T. Dillon, "Geology of Northern Alaska," in *Geology of Alaska*, pp. 49–140, Geological Society of America, 1994, ISBN 0-8137-5219-1.

[40] R. Harris, "Structure and composition of sub-ophiolite metamorphic rocks, western Brooks Range ophiolite belt, Alaska," *Geological Society of America Abstracts with Programs ; Vol. 19*, p. 387, 1987.

[41] R. Harris, "The nature of the Banda Arc-continent collision in the Timor region," in *Arc-Continent Collision*, pp. 163–211, Springer, 2011.

[42] C. W. Hoiland, E. L. Miller, V. Pease, and J. K. Hourigan, "Detrital zircon U-Pb geochronology and Hf isotope geochemistry of metasedimentary strata in the southern Brooks Range: constraints on Neoproterozoic–Cretaceous evolution of Arctic Alaska," *Geological Society, London, Special Publications*, vol. 460, no. 1, pp. 121–158, 2018.

[43] E. L. Miller, K. E. Meisling, V. V. Akinin et al., "Circum-Arctic Lithosphere Evolution (CALE) Transect C: displacement of the Arctic Alaska-Chukotka microplate towards the Pacific during opening of the Amerasia Basin of the Arctic," *Geological Society, London, Special Publications*, vol. 460, no. 1, pp. 57–120, 2018.

[44] W. J. Nokleberg, L. M. Parfenov, J. W. H. Monger et al., "Phanerozoic tectonic evolution of the Circum-North Pacific," *USGS Professional Paper*, 2001.

[45] C. W. Hoiland, E. L. Miller, and V. Pease, "Greenschist facies metamorphic zircon overgrowths as a constraint on exhumation of the Brooks Range metamorphic core, Alaska," *Tectonics*, vol. 37, no. 10, pp. 3429–3455, 2018.

[46] C. J. Warren, R. R. Parrish, D. J. Waters, and M. P. Searle, "Dating the geologic history of Oman's Semail ophiolite: insights from U-Pb geochronology," *Contributions to Mineralogy and Petrology*, vol. 150, no. 4, pp. 403–422, 2005.

[47] R. Crane, "Cretaceous olistostrome model, Brooks Range, Alaska," in *Alaskan North Slope Geology*, vol. 50, pp. 433–440, Pacific Section of Society of Economic Paleontologists and Mineralogists and the Alaska Geological Society, Bakersfield, California, 1987.

[48] F. Cole, K. J. Bird, J. Toro et al., "An integrated model for the tectonic development of the frontal Brooks Range and Colville Basin 250 km west of the Trans-Alaska Crustal Transect," *Journal of Geophysical Research: Solid Earth*, vol. 102, no. B9, pp. 20685–20708, 1997.

[49] T. M. O'Brien, E. L. Miller, V. Pease et al., "Provenance, U-Pb detrital zircon geochronology, Hf isotopic analyses, and Cr-spinel geochemistry of the northeast Yukon-Koyukuk Basin: implications for interior basin development and sedimentation in Alaska," *GSA Bulletin*, vol. 130, pp. 825–847, 2017.

[50] R. Harris, D. Stone, and D. Turner, "Tectonic implications of paleomagnetic and geochronologic data from the Yukon-Koyukuk province, Alaska," *Geological Society of America Bulletin*, vol. 99, no. 3, pp. 362–375, 1987.

[51] A. V. Sobolev, A. W. Hofmann, D. V. Kuzmin et al., "The amount of recycled crust in sources of mantle-derived melts," *Science*, vol. 316, no. 5823, pp. 412–417, 2007.

[52] I. Baziotis, E. Mposkos, and P. Asimow, "Continental rift and oceanic protoliths of mafic-ultramafic rocks from the Kechros Complex, NE Rhodope (Greece): implications from petrography, major and trace-element systematics, and MELTS modeling," *International Journal of Earth Sciences*, vol. 103, no. 4, pp. 981–1003, 2014.

[53] J. A. Pearce and R. J. Stern, "Origin of back-arc basin magmas: trace element and isotope perspectives," *Geophysical Monograph-American Geophysical Union*, vol. 166, p. 63, 2006.

[54] J. Foley, D. C. Dahlin, C. L. Mardock, and W. K. O'Connor, *Reconnaissance investigations of chromite deposits and platinum-group metals in the western Brooks Range, northwestern Alaska*, pp. 80–92, 1992.

[55] P. Pagé, J. H. Bédard, J.-M. Schroetter, and A. Tremblay, "Mantle petrology and mineralogy of the Thetford Mines ophiolite complex," *Lithos*, vol. 100, no. 1-4, pp. 255–292, 2008.

[56] J. A. Pearce, P. Barker, S. Edwards, I. Parkinson, and P. Leat, "Geochemistry and tectonic significance of peridotites from the South Sandwich arc-basin system, South Atlantic," *Contributions to Mineralogy and Petrology*, vol. 139, no. 1, pp. 36–53, 2000.

[57] H.-F. Zhang, "Transformation of lithospheric mantle through peridotite-melt reaction: a case of Sino-Korean craton," *Earth and Planetary Science Letters*, vol. 237, no. 3-4, pp. 768–780, 2005.

[58] I. J. Parkinson and J. A. Pearce, "Peridotites from the Izu-Bonin-Mariana forearc (ODP Leg 125): evidence for mantle melting and melt-mantle interaction in a supra-subduction zone setting," *Journal of Petrology*, vol. 39, no. 9, pp. 1577–1618, 1998.

[59] B. I. McInnes, M. Gregoire, R. A. Binns, P. M. Herzig, and M. D. Hannington, "Hydrous metasomatism of oceanic sub-arc mantle, Lihir, Papua New Guinea: petrology and geochemistry of fluid-metasomatised mantle wedge xenoliths," *Earth and Planetary Science Letters*, vol. 188, no. 1-2, pp. 169–183, 2001.

[60] M. Gavrilenko, C. Herzberg, C. Vidito, M. J. Carr, T. Tenner, and A. Ozerov, "A calcium-in-olivine geohygrometer and its

application to subduction zone magmatism," *Journal of Petrology*, vol. 57, pp. 1811–1832, 2016.

[61] E. Todd, J. B. Gill, and J. A. Pearce, "A variably enriched mantle wedge and contrasting melt types during arc stages following subduction initiation in Fiji and Tonga, southwest Pacific," *Earth and Planetary Science Letters*, vol. 335, pp. 180–194, 2012.

[62] J. A. Pearce and M. K. Reagan, "Identification, classification, and interpretation of boninites from Anthropocene to Eoarchean using Si-Mg-Ti systematics," *Geosphere*, vol. 15, no. 4, pp. 1008–1037, 2019.

[63] R. J. Stern, M. Reagan, O. Ishizuka, Y. Ohara, and S. Whattam, "To understand subduction initiation, study forearc crust: to understand forearc crust, study ophiolites," *Lithosphere*, vol. 4, no. 6, pp. 469–483, 2012.

[64] R. R. Gottschalk, "Petrology of eclogite and associated high-pressure metamorphic rocks, south-central Brooks Range, Alaska," *Special Papers-Geological Society of America*, pp. 141–162, 1998.

[65] R. D. Law, E. L. Miller, T. A. Little, and J. Lee, "Extensional origin of ductile fabrics in the Schist Belt, Central Brooks Range, Alaska—II. Microstructural and petrofabric evidence," *Journal of Structural Geology*, vol. 16, no. 7, pp. 919–940, 1994.

[66] F. H. Wilson, C. P. Hults, C. G. Mull, and S. M. Karl, *Geologic map of Alaska*, US Geological Survey Scientific Investigations Map, 2015.

[67] J. W. Shervais, "Ti-V plots and the petrogenesis of modern and ophiolitic lavas," *Earth and Planetary Science Letters*, vol. 59, no. 1, pp. 101–118, 1982.

[68] R. G. Coleman, *Ophiolites: Ancient Oceanic Lithosphere?*, Springer Verlag, 1977.

[69] T. Ishii, P. T. Robinson, H. Maekawa, and R. Fiske, "Petrological studies of peridotites from diapiric serpentinite seamounts in the Izu-Ogasawara-Mariana forearc, Leg 125," *Proceedings of the Proceedings of the Ocean Drilling Program, Scientific Results*, , Ocean Drilling Program, College Station, 1992.

[70] H. A. Gahlan, M. K. Azer, P. D. Asimow, and K. M. Al-Kahtany, "Genesis and geodynamic evolution of serpentinized ultramafics and associated magnesite deposits in the Al-Wask ophiolite, Arabian Shield, Saudi Arabia," *American Journal of Science*, vol. 320, no. 3, pp. 236–279, 2020.

[71] S.-S. Sun and W. F. McDonough, "Chemical and isotopic systematics of oceanic basalts: implications for mantle composition and processes," *Geological Society, London, Special Publications*, vol. 42, no. 1, pp. 313–345, 1989.

[72] M. Grégoire, B. I. McInnes, and S. Y. O'Reilly, "Hydrous metasomatism of oceanic sub-arc mantle, Lihir, Papua New Guinea: part 2. Trace element characteristics of slab-derived fluids," *Lithos*, vol. 59, pp. 91–108, 2001.

[73] D. A. Ionov, "Petrology of mantle wedge lithosphere: new data on supra-subduction zone peridotite xenoliths from the andesitic Avacha Volcano, Kamchatka," *Journal of Petrology*, vol. 51, no. 1-2, pp. 327–361, 2010.

[74] I. Parkinson, R. Arculus, and S. Eggins, "Peridotite xenoliths from Grenada, Lesser Antilles island arc," *Contributions to Mineralogy and Petrology*, vol. 146, no. 2, pp. 241–262, 2003.

[75] R. Vannucci, M. Tiepolo, M. Defant, and P. Kepezhinskas, "The metasomatic record in the shallow peridotite mantle beneath Grenada (Lesser Antilles arc)," *Lithos*, vol. 99, no. 1-2, pp. 25–44, 2007.

[76] W. K. Conrad and R. W. Kay, "Ultramafic and mafic inclusions from Adak Island: crystallization history, and implications for the nature of primary magmas and crustal evolution in the Aleutian Arc," *Journal of Petrology*, vol. 25, no. 1, pp. 88–125, 1984.

[77] S. Debari, S. M. Kay, and R. Kay, "Ultramafic xenoliths from Adagdak volcano, Adak, Aleutian Islands, Alaska: deformed igneous cumulates from the Moho of an island arc," *The Journal of Geology*, vol. 95, no. 3, pp. 329–341, 1987.

[78] F. Calabozo, J. Strelin, R. Keller, J. Brod, and F. Fuentes-Iza, "Mantle xenoliths from James Ross Island, Antarctic Peninsula: a preliminary whole-rock and mineral chemistry study," *XIX Congreso Geológico Argentino*, pp. T8–11, 2014.

[79] Ş. Altunkaynak, A. Ünal, G. H. Howarth, E. Aldanmaz, and D. Nỳvlt, "The origin of low-Ca olivine from ultramafic xenoliths and host basaltic lavas in a back-arc setting, James Ross Island, Antarctic Peninsula," *Lithos*, vol. 342, pp. 276–287, 2019.

[80] Y. Ichiyama, T. Morishita, A. Tamura, and S. Arai, "Peridotite xenoliths from the Shiribeshi Seamount, Japan Sea: insights into mantle processes in a back-arc basin," *Contributions to Mineralogy and Petrology*, vol. 171, p. 86, 2016.

[81] A. Sanfilippo, R. Tribuzio, and M. Tiepolo, "Mantle-crust interactions in the oceanic lithosphere: constraints from minor and trace elements in olivine," *Geochimica et Cosmochimica Acta*, vol. 141, pp. 423–439, 2014.

[82] S. A. Dare, J. A. Pearce, I. McDonald, and M. T. Styles, "Tectonic discrimination of peridotites using fO_2-Cr# and Ga-Ti-Fe^{III} systematics in chrome-spinel," *Chemical Geology*, vol. 261, no. 3-4, pp. 199–216, 2009.

[83] S. Arai and S. Ishimaru, "Insights into petrological characteristics of the lithosphere of mantle wedge beneath arcs through peridotite xenoliths: a review," *Journal of Petrology*, vol. 49, pp. 665–695, 2008.